Composite Structures 305 (2023) 116482

Contents lists available at ScienceDirect

Composite Structures

journal homepage: www.elsevier.com/locate/compstruct

In-plane mechanical properties of a novel cellular structure for morphing applications

Ting Li [a], Jian Sun [b], Jinsong Leng [b], Yanju Liu [a,*]

[a] Department of Astronautical Science and Mechanics, Harbin Institute of Technology (HIT), P.O.Box 301, No. 92 West Dazhi Street, Harbin 150001, People's Republic of China

[b] Center for Composite Materials and Structures, Science Park of Harbin Institute of Technology (HIT), P.O. Box 3011, No. 2 YiKuang Street, Harbin 150080, People's Republic of China

ARTICLE INFO

Keywords:
Cellular structure
Three-dimensional deformation
zero Poisson's ratio
Elastic modulus

ABSTRACT

Cellular structures provide outstanding mechanical characteristics such as low density, zero Poisson's ratio, and out-of-plane bearing capacity, displaying their extensive application prospects as a supporting framework for flexible morphing skins. Unlike traditional cellular structures that produce two-dimensional deformation under in-plane loading, this work proposes a novel cellular structure that generates local three-dimensional deformation activated by in-plane tension. The designed topology evolves from accordion honeycomb by tilting an angle of the inclined cell walls. The equivalent in-plane tensile modulus, shear modulus, and local out-of-plane deformation are theoretically deduced considering three-dimensional internal forces existing in the inclined cell walls. The finite element simulations are established, and the corresponding experimental tests are carried out to validate the rationality of the analyzed results. Then the effects on mechanical performance versus geometric parameters of the unit cell are investigated, and the theoretical and simulated results illustrate good agreement generally.

1. Introduction

Morphing skin is one of the crucial technologies to achieve the dynamic deformation of aircraft flying like a bird, which should meet the demands of flexibility to deform and stiffness to bear aerodynamic loads simultaneously[1,2]. The adaptive cellular structure covered with flexible silicone rubber skin is a feasible scheme for morphing skin, with low stiffness to morph and high stiffness to withstand the out-of-plane load. Olympio et al. investigated several morphing skins that used high-strain capable and high bending stiffness cellular cores with low modulus facesheets covered for in-plane uniaxial and shearing morphing[3–6]. Bubert et al. designed a passive elastomeric matrix composite morphing skin supported by a honeycomb structure with zero Poisson's ratio and demonstrated 100% uniaxial extension with potential for span-morphing UAV wingtip[7]. These studies show that cellular structures covered with flexible external skin have a promising application for morphing skins, stimulating extensive research on cellular supportive structures.

Cellular structures exhibit light weight and remarkable mechanical properties related to the topology and geometric size of cells and have been widely investigated by combining theoretical, simulation, and experimental methods. Many research works on cellular structures with a positive, negative, or zero Poisson's ratio value have been conducted [8–12]. Cellular structures with various topologies have been proposed, such as accordion cellular structure composed of elastic beams for one-dimensional deformation[13,14], star-shaped cells for two-dimensional shearing morphing[15–17], sandwich honeycomb composed of hexagonal components and thin plates[18,19], chiral honeycombs and anti-tetrachiral honeycombs[20–23], re-entrant honeycombs[24,25] and hybrid-honeycomb structures[26–29]. When suffering in-plane load in one direction, zero Poisson's ratio honeycombs will neither shrink nor expand in the orthogonal direction. In addition, when these honeycombs bear out-of-plane bending loads, neither anticlastic curvature like positive Poisson's ratio honeycombs nor synclastic curvature like negative Poisson's ratio honeycombs will occur. These properties make honeycombs with zero Poisson's ratio more suitable for morphing wings [6,15,30]. However, the cellular structures cannot provide active morphing, so they need additional actuators to drive adaptive deformation. Shape memory alloy (SMA) actuators, including wires and springs, are ideal candidates to actuate morphing wings for their high

* Corresponding author.
E-mail address: yj_liu@hit.edu.cn (Y. Liu).

https://doi.org/10.1016/j.compstruct.2022.116482
Received 25 May 2021; Received in revised form 15 September 2022; Accepted 14 November 2022
Available online 17 November 2022

energy density and large driving forces[31–34]. If stimulated by temperature, SMA undergoes a phase transition and responds quickly to restore the original shape from the deformed state. By stimulating SMA actuators to contract along the chord direction, morphing wings are driven to deform. This deformation mechanism may require a larger size or a reasonable spatial layout of SMA actuators. A novel deformable structure called KinetiX constructed by rigid plates and elastic hinges was proposed. One of the combinations demonstrates the characteristics of large bending deformation under in-plane load[35]. Although the flexible hinges allow KinetiX to exhibit large bending deformation, the deformed bending state cannot be fixed to bear aerodynamic loads, limiting the application in morphing wings.

This project aims to design active morphing skin supported by cellular structures and actuating by SMA actuators to drive bending deformation for morphing camber wings. This work presents the first part: developing a novel cellular structure as a potential supportive core for flexible skin and analyzing the in-plane mechanical properties. The novel cellular structure is obtained by turning the cell wall over an angle to deviate from the plane perpendicular to the honeycomb. This design method maintains the geometric hexagonal configuration and makes cell walls generate out-of-plane internal forces to induce 3D deformation when uniaxial tension is applied. The designed honeycomb is a planar structure that exhibits local three-dimensional deformation and shows zero Poisson's ratio when subjected to in-plane tensile load. Theoretical analysis is developed to obtain the in-plane tensile elastic modulus and equivalent shear modulus of the 3D deformed honeycomb structure. The out-of-plane displacement under stretching is calculated. The rationality of the analytic results is verified by finite element (FE) simulation and experimental tests. The effects of geometrical parameters on the in-plane stiffness are also discussed by theoretical analysis and FE simulation.

2. Models and experimental tests

2.1. Geometry of the designed honeycomb structure

Fig. 1a shows the geometric model of the designed 3D deformed honeycomb. It is evident that the honeycomb exhibits periodicity in both horizontal and vertical directions. A representative cell is selected for analysis, as shown in Fig. 1b, Fig. 1c. The following three parts can describe the representative cell: 1) the hexagonal inclined cell wall perpendicular to the honeycomb plane; 2) the hexagonal inclined cell wall with an angle to the honeycomb plane; 3) the horizontal cell wall connects both inclined walls. The unit cell exhibits symmetry in both horizontal and vertical directions. The lengths of the three cell walls described above are expressed by parameters βl, αl, and l, respectively. The thickness and depth of inclined and horizontal walls are represented by parameters t, λt, and b. They are expressed by $t = \xi l$ and $b = \zeta l$ to obtain a non-dimensional description of the honeycomb unit cell. The parameter φ stands for the internal cell angle, while θ symbolizes the tilt angle between inclined walls and the plane perpendicular to the honeycomb. The width of the unit cell is ηl, and the height is $h = 2l[(\alpha+\beta)\cos\varphi + \lambda\xi]$. When setting different parameters to construct the cell configurations, the following geometric constraints should be satisfied to avoid contacts or intersections between adjacent cell walls:

$$\begin{cases} \zeta\tan\theta < \dfrac{1}{2} \\ \eta - \dfrac{2\xi}{\cos\varphi} - 1 > \{2\alpha\sin\varphi, 2\beta\sin\varphi\}_{\max} \end{cases} \tag{1}$$

2.2. Theoretical model

When applying tensile loads to the honeycomb along the x direction, the horizontal cell walls bear tensile loads without causing the deformation of the inclined cell walls. Therefore, the honeycomb deformation

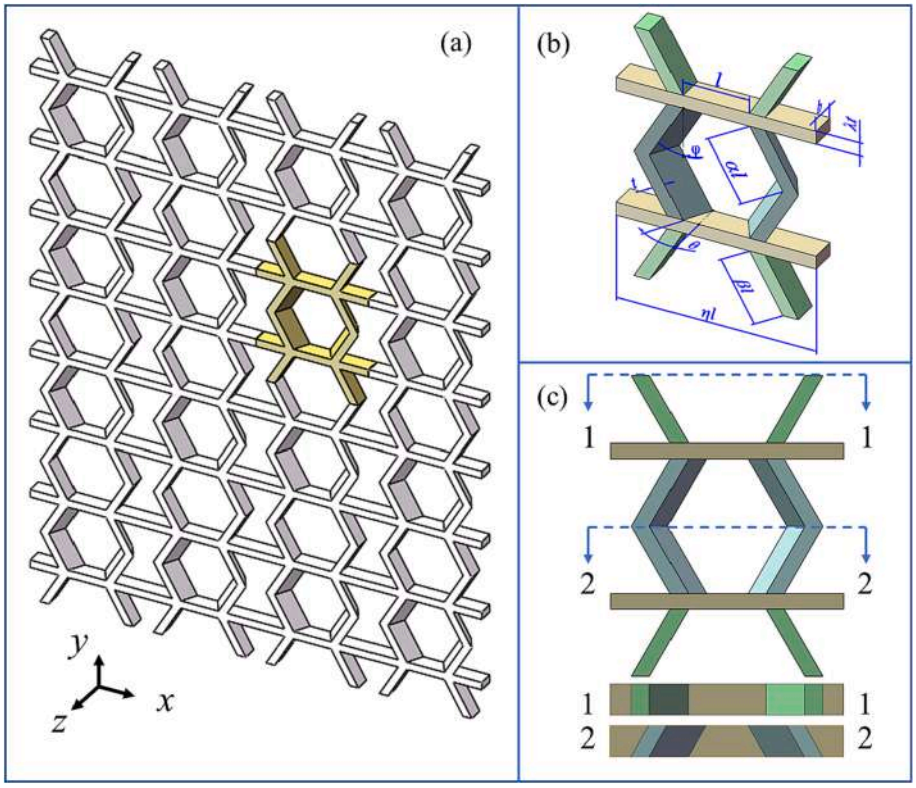

Fig. 1. The geometric configuration of cellular structure with zero Poisson's ratio: (a) 3D model, (b) representative cell with geometric representations, (c) front view, bottom view and section view.

in the y direction will not occur when loaded in the x direction. This feature can be summarized as the in-plane Poisson's ratio ν_{xy} of the 3D deformed honeycomb structure is zero. When applying tensile loads to the honeycomb along the y direction, the inclined cell walls bend and cause global elongation deformation of the honeycomb. In addition, the honeycomb structure is symmetrical, and the elongation or shortening of the horizontal cell walls will not occur without external force in the x direction, so ν_{yx} is also considered zero through analysis.

Castigliano's second theorem is adopted in this work to derivate the equivalent elastic modulus among horizontal (x) and vertical (y) directions. Here assumes that the honeycomb cell walls undergo flexural and axial deformation during the theoretical calculation while ignoring the relatively small shear and torsion deformation. Castigliano's second theorem is described as follows: the strain energy U of the elastic system is expressed as a function of any applied force P_i, and the partial derivative with respect to P_i of the strain energy U is equal to the displacement δ_i along the loading direction of P_i:

$$\frac{\partial U}{\partial P_i} = \delta_i \tag{2}$$

2.2.1. Equivalent tensile modulus in the x direction

The loading scheme of the unit cell for calculating the equivalent modulus in the x direction is shown in Fig. 2. The slight out-of-plane deformation of the inclined cell walls caused by in-plane forces is not considered when loading in the x direction. The deformation of the hexagonal inclined cell walls is ignored, for it hardly affects the overall deformation of the honeycomb along the loading direction. Therefore, the equivalent tensile modulus in the x direction can be solved by finding the homogenization stress and strain. Due to the horizontal and vertical symmetry of the cell, the stress of a quarter cell is analyzed. The displacement of the horizontal cell wall with a rectangular cross-section under tension can be obtained as:

$$\delta_x = \frac{F\eta}{2E_s\lambda\xi\zeta l} \tag{3}$$

Where E_s is the elastic modulus of the raw material of the 3D deformed honeycomb, the homogenization strain and stress under horizontal tension are accessed as follows:

$$\varepsilon_x = \delta_x \Big/ \frac{\eta l}{2} = \frac{F}{E_s\lambda\xi\zeta l^2} \tag{4}$$

$$\sigma_x = \frac{F}{[(\alpha+\beta)\cos\varphi + \lambda\xi]\zeta l^2} \tag{5}$$

The non-dimensional and homogenized equivalent Young's modulus along the x direction equals the ratio of stress divided by strain:

$$\frac{E_x}{E_s} = \frac{\lambda\xi}{[(\alpha+\beta)\cos\varphi + \lambda\xi]} \tag{6}$$

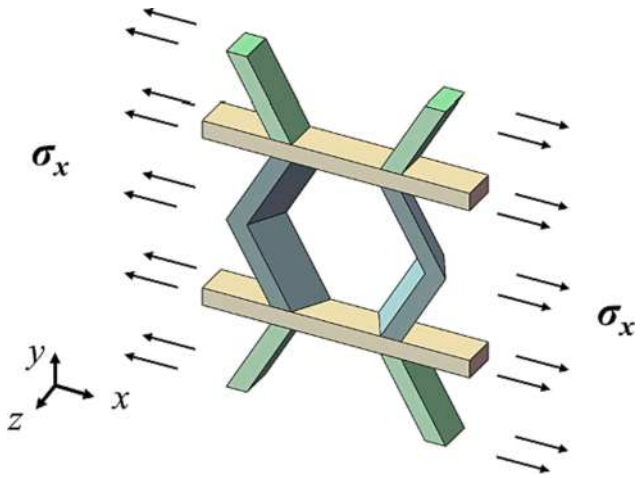

Fig. 2. Theoretical calculation model of tensile modulus in x direction.

2.2.2. Equivalent tensile modulus in the y direction

Fig. 3 shows the loading scheme for analyzing elastic modulus along the y direction of the designed 3D deformed honeycomb structure. The geometric shape of the honeycomb unit cell is horizontally symmetrical, vertically symmetrical, and centrally symmetrical. When the uniform load is applied in the y direction, it mainly acts on the oblique cell wall. The deformation of the horizontal cell wall is not considered. Fig. 3b shows a schematic diagram of the unit cell subjected to the uniform tensile load in the y direction and the force analysis of a quarter cell, where the Cartesian coordinate system x-y-z is the global coordinate system, and x_1-y-z_1 is the local coordinate system. The model is divided into two parts, the inclined hexagonal cell wall with an angle from the perpendicular plane (plane yz) above the horizontal wall and the hexagonal oblique cell wall perpendicular to the surface below.

In this work, the counter-clockwise direction is defined as the positive direction of the bending moment, and the tensile direction of the cell wall is recognized as the positive direction of axial force. It is worth noting that M_x, M_z, M_{x1}, and M_{z1} are all unknown bending moments related to the force F. Due to the horizontal symmetry of the honeycomb cell, the upper and lower surfaces of the quarter cell structure have no angular displacement around the x and z directions. Therefore, the following boundary conditions can be obtained:

$$\frac{\partial U_{down}}{\partial M_x} = 0,\ \frac{\partial U_{down}}{\partial M_z} = 0,\ \frac{\partial U_{up}}{\partial M_{x1}} = 0 \text{ and } \frac{\partial U_{up}}{\partial M_{z1}} = 0 \tag{7}$$

The simplified walls are subjected to in-plane flexural internal force $M_z(s)$, out-of-plane bending internal force $M_x(s)$ and axial load $F_N(s)$. The elastic strain energy U is expressed by:

$$U = \int \frac{F_N^2(s)}{2E_sA}ds + \int \frac{M_z^2(s)}{2E_sI_z}ds + \int \frac{M_x^2(s)}{2E_sI_x}ds \tag{8}$$

Where E_s is Young's modulus of the substrate material, and A, I_x and I_z are the cross-sectional area of the inclined cantilever beam, the section moment of inertia on the x-axis and the section moment of inertia on the z-axis, respectively. According to the equilibrium equation of the honeycomb cell wall, the internal force and moment distribution at any section of the upper inclined cell wall can be described as follows:

$$\begin{aligned} &F_N = F,\ M_{x1}(s) = -M_{x1} + Fs\sin\varphi\sin\theta, \\ &M_{z1}(s) = -M_{z1} + Fs\sin\varphi\cos\theta,\ 0 \leqslant s \leqslant \alpha l \end{aligned} \tag{9}$$

The cross-sectional shape of the upper inclined cell wall is a parallelogram, and the cross-sectional characteristics are solved:

$$A_1 = \xi\zeta l^2,\ I_{x1} = \frac{l^4\xi\left(2\xi^3\sin^3 2\theta - 3\xi^2\zeta\sin^2 2\theta + 4\zeta^3\right)}{48\cos^2\theta} \text{ and } I_{z1} = \frac{\xi^3\zeta\cos^2\theta}{12}l^4 \tag{10}$$

For the inclined cell wall with a rectangular cross-section below the horizontal cell wall, the internal force distribution and the section properties are:

$$F_N = F\cos\varphi,\ M_x(s) = -M_x,\ M_z(s) = -Fs\sin\varphi - M_z,\ 0 \leqslant s \leqslant \beta l \tag{11}$$

$$A = \xi\zeta l^2,\ I_x = \frac{\xi\zeta^3}{12}l^4 \text{ and } I_z = \frac{\xi^3\zeta}{12}l^4 \tag{12}$$

Next, the expression of strain energy U can be solved by substituting Eq.(9)-(12) into Eq.(8):

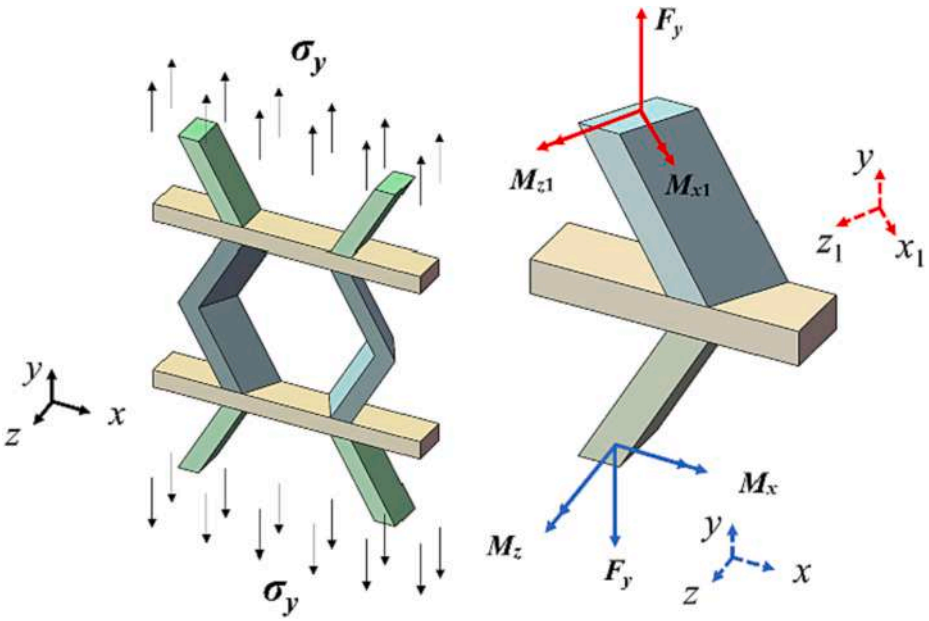

Fig. 3. Analysis models with the loading scheme along the y direction: (a) unit cell; (b)1/4 cell.

$$U = \frac{F^2(\alpha+\beta)\cos^2\varphi}{2E_s\xi\zeta l} + \frac{2\beta\left(F^2\beta^2 l^2\sin^2\varphi + 3FM_z\beta l\sin\varphi + 3M_z^2\right)}{E_s\xi^3\zeta l^3} + \frac{6M_x^2\beta}{E_s\xi\zeta^3 l^3} + \frac{8\alpha\cos^2\theta\left(F^2\alpha^2 l^2\sin^2\varphi\sin^2\theta - 3F\alpha l M_{x1}\sin\varphi\sin\theta + 3M_{x1}^2\right)}{E_s\xi l^3\left(2\xi^3\sin^3 2\theta - 3\xi^2\zeta\sin^2 2\theta + 4\zeta^3\right)} + \frac{6M_{z1}^2\alpha + 2F^2\alpha^3 l^2\cos^2\theta\sin^2\varphi - 6FM_{z1}\alpha^2 l\cos\theta\sin\varphi}{E_s\xi^3\zeta l^3\cos^2\theta} \tag{13}$$

Combining the previous solution results and the boundary conditions of Eq.(7) to find the relationship between the unknown bending moment and F:

$$M_{x1} = \frac{F\alpha l\sin\varphi\sin\theta}{2},\ M_{z1} = \frac{F\alpha l\sin\varphi\cos\theta}{2},\ M_x = 0,\ M_z = -\frac{F\beta l\sin\varphi}{2} \tag{14}$$

Integrating Eq.(2), it is natural to acquire the vertical displacement of the free top surface under uniform tensile force in the y direction:

$$\delta_y = \frac{F(\alpha+\beta)\cos^2\varphi}{E_s l\xi\zeta} + \frac{F\left(\alpha^3+\beta^3\right)\sin^2\varphi}{E_s l\xi^3\zeta} + \frac{F\alpha^3\zeta\sin^2\varphi}{E_s l\xi\rho}$$
$$\rho = 4\xi^3\cos\theta\sin\theta - 3\xi^2\zeta + \frac{\zeta^3}{\cos^2\theta\sin^2\theta} \tag{15}$$

Then the homogenization stress and strain along the y direction are denoted as follows:

$$\begin{cases} \sigma_y = \dfrac{2F}{\zeta\eta l^2} \\ \varepsilon_y = \dfrac{\delta_y}{l[(\alpha+\beta)\cos\varphi + \lambda\xi]} \end{cases} \tag{16}$$

Finally, the expression of the homogenized non-dimensional equivalent Young's modulus in the y direction is obtained from dividing the stress by the strain:

$$\frac{E_y}{E_s} = \frac{2\xi[(\alpha+\beta)\cos\varphi + \lambda\xi]/\eta}{(\alpha+\beta)\cos^2\varphi + \frac{\left(\alpha^3+\beta^3\right)\sin^2\varphi}{\xi^2} + \frac{\alpha^3\zeta\sin^2\varphi}{\rho}} \tag{17}$$

2.2.3. In-plane shear modulus

A uniform distributed shear stress is applied to the honeycomb surface to investigate the shear modulus of the 3D deformed cellular structure, as shown in Fig. 4. The honeycomb structure exhibits anti-symmetric under pure shear stress. Therefore, only anti-symmetric shear force exists in the symmetry plane, and symmetrical internal forces such as axial force and bending moment are zero. In this section, the deformation of a quarter model of the representative cell is analyzed similarly, regardless of the bending moment M_x caused by the horizontal cell wall and the torque T in the inclined cell wall. It is easy to get the

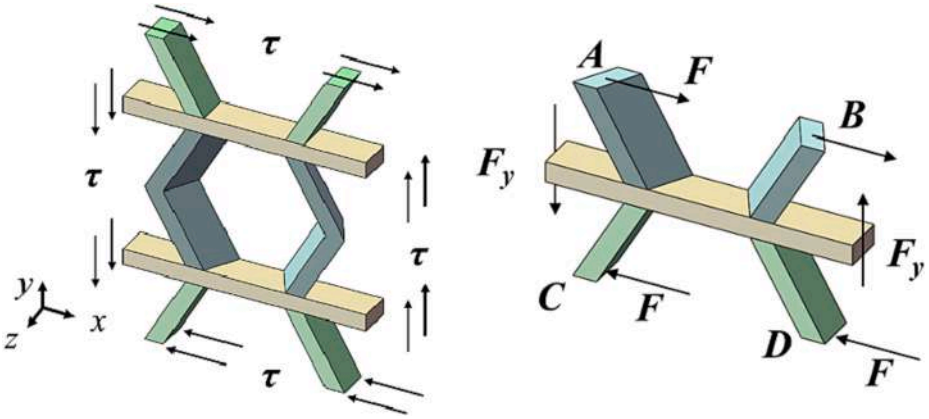

Fig. 4. Unit cell bearing in-plane shear stress.

equilibrium equation expressed by force F and shear stress τ through the force analysis of the cell:

$$F[\lambda\xi + (\alpha+\beta)\cos\varphi] = F_y\eta,\ F = \frac{\tau\eta\zeta l^2}{2} \tag{18}$$

Due to the bisymmetry of the model, no horizontal relative displacement occurs between the two points AB, nor does CD. The shear deformation of the semi-model under the applied uniform shear stress can be simplified into two parts: the relative horizontal displacement of points AC and the relative vertical displacement between points AB. Therefore, the equivalent shear strain can be given by the ratio of displacement to the geometric length of the model:

$$\gamma = \frac{u_{xA} - u_{xC}}{[\lambda\xi + (\alpha+\beta)\cos\varphi]l} + \frac{2u_{yA}}{\eta l} \tag{19}$$

Where u_{xA} and u_{xC} are the horizontal displacements of the two inclined walls under shear stress, respectively. The internal force distribution of inclined wall above the horizontal cell wall in a local coordinate system bearing shear force F and a unit force along the positive x is as follows:

$$\begin{aligned} &F_N = -F\sin\varphi,\ M_{x1}(s) = Fs\cos\varphi\sin\theta,\\ &M_{z1}(s) = Fs\cos\varphi\cos\theta,\ 0\leqslant s\leqslant\alpha l \end{aligned} \tag{20}$$

$$\overline{F_N} = -\sin\varphi,\ \overline{M_{x1}}(s) = s\cos\varphi\sin\theta,\ \overline{M_{z1}}(s) = s\cos\varphi\cos\theta,\ 0\leqslant s\leqslant\alpha l \tag{21}$$

$$\overline{F}_N^{'} = \cos\varphi, \overline{M}_{z1}^{'}(s) = ssin\varphi\sin\theta, \overline{M}_{z1}^{'}(s) = ssin\varphi cos\theta, 0 \le s \le \alpha l \tag{22}$$

The horizontal displacement and vertical of the top end of the inclined rod are calculated by Mohr integral:

$$u = \int_0^L \frac{F_N(s)\overline{F_N}(s)}{EA}ds + \int_0^L \frac{M_x(s)\overline{M_x}(s)}{EI_x}ds + \int_0^L \frac{M_z(s)\overline{M_z}(s)}{EI_z}ds \tag{23}$$

$$u_{xA} = \frac{F\alpha\sin^2\varphi}{E_s l\xi\zeta} + \frac{4F\alpha^3\cos^2\varphi}{E_s l\xi^3\zeta} + \frac{4F\alpha^3\cos^2\varphi}{E_s l\xi\rho} \tag{24}$$

$$u_{yA} = \frac{4F\alpha^3\sin\varphi\cos\varphi}{E_s l\xi^3\zeta} - \frac{F\alpha\sin\varphi\cos\varphi}{E_s l\xi\zeta} + \frac{4F\alpha^3\sin\varphi\cos\varphi}{E_s l\xi\rho} \tag{25}$$

The horizontal displacement of the end of the inclined rod below the horizontal cell wall can be written by repeating the above steps as follows:

$$u_{xC} = -\frac{F\beta\sin^2\varphi}{E_s l\xi\zeta} - \frac{4F\beta^3\cos^2\varphi}{E_s l\xi^3\zeta} \tag{26}$$

Combing with Eq.(18) (19) and $G = \tau/\gamma$, the non-dimensional equivalent homogenized shear modulus G/E_s can be obtained.

2.2.4. Out-of-plane deformation

The proposed cellular structure can activate out-of-plane deformation under tensile load, which is quantitatively analyzed below. It is worth mentioning that a spatial geometric relationship exists and makes the given tilt angle of the inclined cell wall differ from the angle in the theoretical analysis. When analyzing the equivalent modulus, this difference has little effect on the equivalent modulus and is therefore ignored. However, the angle difference cannot be overlooked when analyzing the out-of-plane deformation, so the relationship between the two angles needs to be determined first. The angle between the hypotenuse on the plane perpendicular to the inclined wall and z axis is defined as ψ. From the spatial geometric relationship, the following expression can be obtained:

$$\frac{\tan\theta}{\cos\varphi} - \tan\psi - \tan\varphi\sqrt{\frac{1}{\cos^2\theta} - \frac{1}{\cos^2\psi}} = 0 \tag{27}$$

According to the solution process in section 3.3, the internal force distribution of the inclined hexagonal cell wall that has an angle with the honeycomb plane is:

$$\begin{aligned} &F_N = F\cos\varphi,\ M_{x1}(s) = F\left(s - \frac{\alpha l}{2}\right)\sin\varphi\sin\psi,\\ &M_{z1}(s) = F\left(s - \frac{\alpha l}{2}\right)\sin\varphi\cos\psi,\ 0\leqslant s\leqslant\alpha l \end{aligned} \tag{28}$$

Obtain out-of-plane deformation through coordinate transformation:

$$u_z = u_{z1}\cos\psi + u_{x1}\sin\psi \tag{29}$$

Where u_{x1} and u_{z1} represent the displacement along the x_1 and z_1 axis under tensile load F along the y axis in the local coordinate system x_1-y-z_1, respectively, which are analyzed by the unit force method in the following text. The out-of-plane deformation of the honeycomb unit cell along axis z_1 caused by stretching in the y direction can be obtained:

$$\begin{aligned} u_{z1} &= \int_0^{\alpha l} \frac{F(s-\alpha l/2)\sin\varphi\sin\psi}{E_s I_{x1}}\cdot(-s)ds\\ &= -\frac{F\alpha^3\sin\varphi\sin\psi}{E_s l\left(4\xi^4\cos\psi\sin^3\psi - 3\xi^3\zeta\sin^2\psi + \frac{\xi\zeta^3}{\cos^2\psi}\right)} \end{aligned} \tag{30}$$

Similarly, applying a unit force along the x_1 direction to the free end of the inclined cell wall to obtain:

$$u_{x1} = \frac{F\alpha^3\sin\varphi}{E_s l\xi^3\zeta\cos\psi} \tag{31}$$

Following Eq.(29) to obtain out-of-plane deformation under uniaxially stretched along y direction:

$$\begin{aligned} u_z &= \frac{F\alpha^3\sin\varphi\sin\psi\left(\omega_2 - \xi^2\zeta\cos^4\psi - \omega_1 + \zeta^3\right)}{E_s l\xi^3\zeta\cos\psi\left(\omega_2 - \omega_1 + \zeta^3\right)}\\ \omega_1 &= 3\xi^2\zeta\cos^2\psi\sin^2\psi\\ \omega_2 &= 4\xi^3\cos^3\psi\sin^3\psi \end{aligned} \tag{32}$$

2.3. Finite element simulation

In this work, commercial finite element software Abaqus (2016, Abaqus Inc.) was used to analyze the numerical homogenized in-plane modulus. The full-scale representative honeycomb with 4 x 4 cells, as shown in Fig. 5, was established to calculate the numerical equivalent tensile modulus along the x and y directions and the equivalent shear modulus. The 3D models were developed using linear hexahedral element (C3D8R) defined by 8 nodes and six degrees of freedom at each node. After a convergence test, the minimum global mesh density was 0.75 mm, the element size of wall thickness was $t/2$, and the number of elements obtained by this setup was about 30 thousand. The boundary conditions of the three categories are listed in Table 1[18]. It is worth noting that the symbols ε_0 and γ_0 here represent the imposed tensile and shear strain, respectively, and L_i ($i = x$ or y) represents the total length of the full-scale honeycomb structure along i direction. The displacement constraint was applied to the master node built at the center of the loading surface coupled with all nodes. The homogenized stresses were calculated by averaging the reaction forces of the master node over the area of the loading surface. Then the equivalent moduli were obtained as the ratios of the averaged stresses to the imposed strains.

2.4. Honeycomb preparation and experiment

All specimens of the 3D deformed honeycomb were prepared by a rapid prototyping 3D printer (ANICUBIC mega) based on the fusion deposition molding (FDM) technique with polylactic acid (PLA) plastic. The 3D printer has a 0.4 mm diameter brass nozzle, using PLA filaments with 1.75 mm diameter to fabricate specimens. Depending on the 3D printer and the material properties of PLA, the platform temperature and extrusion nozzle temperature were set to 60 °C and 200 °C, respectively,

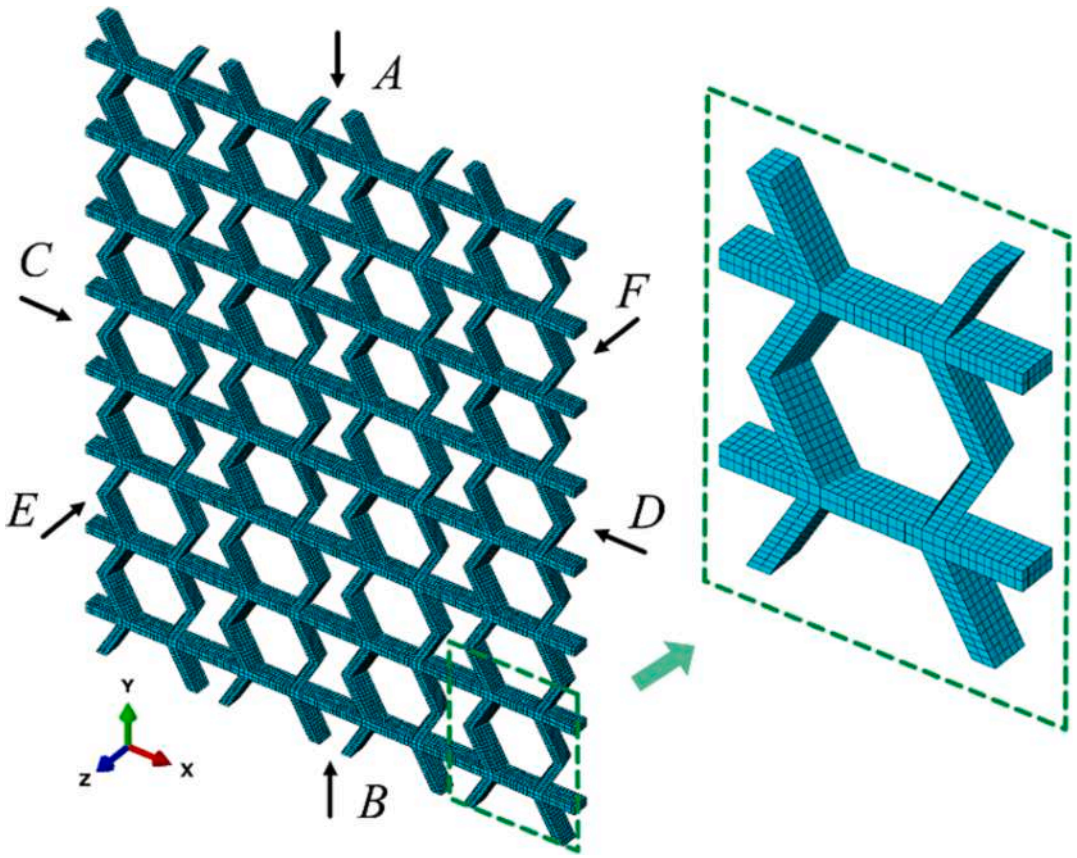

Fig. 5. FE simulation model of in-plane tensile modulus.

Table 1
The setting of boundary conditions for simulation.

Surface	E_x	E_y	G_{yx}
A	Free	$u_i = 0\ (i = 1\cdots6,\ i \neq 2)$ $u_2 = \varepsilon_0 L_y$	$u_i = 0\ (i = 2\cdots6)$ $u_1 = \gamma_0 L_y$
B	Free	$u_i = 0\ (i = 1\cdots6)$	$u_i = 0\ (i = 1\cdots6)$
C	$u_i = 0\ (i = 1\cdots6)$	Free	Anti-symmetry
D	$u_1 = \varepsilon_0 L_x$ $u_i = 0\ (i = 2\cdots6)$	Free	Anti-symmetry
E	Free	Free	Free
F	Free	Free	Free

to achieve good adhesion and avoid warpage. All honeycombs were printed with a nozzle speed of 60 mm/s in a rectilinear pattern and 0.2 mm layer thickness with 100% infill. For obtaining the mechanical elastic constants of the core material, quasi-static tension tests have been conducted following the ASTM standard (ASTM D638), using Zwick 010 test machine with dumbbell-shaped samples. Similarly, the dumbbell-shaped specimens were prepared by the same 3D printer with constant parameters. The elastic properties of PLA raw material achieved by tensile tests are $E_s = 2069$ MPa, $\nu_s = 0.35$, and $G_s = 766$ MPa, and they were used as the equivalent isotropic mechanical constants in the theoretical calculation and FE simulation.

The in-plane equivalent elastic constants of the 3D deformed cellular structures were tested in this section. Homogenized elastic modulus E_x, E_y, and equivalent shear modulus G_{yx} were characterized by Zwick Z010 tensile machine with 1 kN load cell. Displacement controlled the loading rate and remained constant, with a stretching rate of 2 mm/min along the *x* direction. The loading rate was 5 mm/min for stretching along the *y* direction and applying shear force. Loads were output by force transducers, and position changes of machine crosshead were regarded as displacements. Then stress–strain curves were converted by load–displacement curves to fit the in-plane elastic constant. The homogenized elastic moduli of the 3D deformed honeycomb structures with different cell wall thicknesses were tested. The geometrical unit cell parameters of the 3D deformed honeycomb samples used in the in-plane tensile and shear test are set as follows: $l = 10$ mm, $\alpha = \beta = 1$, $\lambda = 1$, $\eta = 3$, $\zeta = 0.4$, $\varphi = 30^\circ$, $\theta = 15^\circ$, $\xi = 0.12, 0.17, 0.22$. The overall dimensions of the honeycomb samples are shown in Table 2.

When testing the shear modulus G_{yx} of the 3D deformed cellular structure, different from an off-axial test along 45° following the ASTM D3518/ D3518M-13 standard[18], this work performed the shear test by the designed L-shaped clamps that transform loading direction[36]. Due to the angle between inclined cell walls and the honeycomb surface, the 3D deformed honeycomb was no longer uniform along the *z* direction, leading to inconsistent equivalent shear modulus of the selected samples with different dimensions under off-axial 45° tension. Fig. 6 shows the L-shaped clamps capable of measuring the force–displacement response in the deformed direction and eliminating the influence of the honeycomb samples being wider than the grips. The shear modulus can be tested by rotating the clamps by 90°.

The local out-of-plane deformation of the honeycomb specimen induced by in-plane uniaxial tension was measured by a laser displacement sensor (Panasonic HG-C1050) with a range of 30 mm and an accuracy of 30 μm. Fix the laser displacement sensor on the slider for unrestricted movement in the frame constructed with aluminum

Table 2
Dimension of specimens for tensile and shear tests.

Thickness(t)/mm	1.2	1.7	2.2
Stretched along *x*	120 × 77 × 4 mm^3	120 × 75 × 4 mm^3	120 × 73 × 4 mm^3
Stretched along *y* or shear	150 × 90 × 4 mm^3	153 × 90 × 4 mm^3	156 × 90 × 4 mm^3

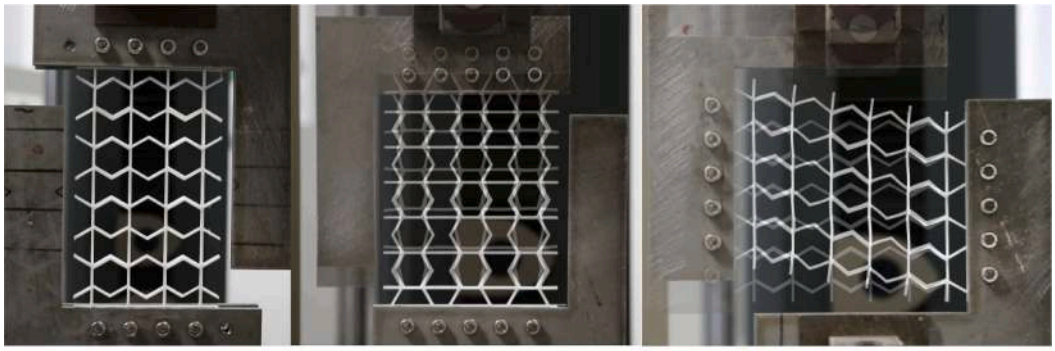

Fig. 6. Experimental setup for in-plane elastic constants: (a)stretched along x direction, (b) stretched along y direction, (c) shear test.

profiles. Before testing the deformation along the z direction, the slider movement plane was calibrated to be parallel to the tensile specimen. The experiments tested three samples with geometric characteristics as follows: $l = 10$ mm, $\alpha = \beta = 1$, $\lambda = 1$, $\eta = 3$, $\zeta = 0.2$, $\varphi = 30°$, $\theta = 30°$, $\xi = 0.12$. The step loading method was used to stretch the samples along the y direction at a rate of 1 mm/min until the load increased to 20 N. When load increased at each interval by 5 N, the upward stretching was stopped and maintained for 180 s to record the deformation read by the laser sensor. As shown in Fig. 7, the relative displacement between points A and B was recognized as the out-of-plane deformation.

3. Results and discussions

Table 3 lists the results of theoretical calculation, experimental tests, and FE simulation with different cell walls' thicknesses, as well as the comparison of the three. For the homogenized tensile elastic modulus E_x, there is a 2.78% discrepancy between the theoretical and the experimental result when $\xi = 0.22$, which is 2.11% lower than the predicted simulated value, and the latter being 0.66% stiffer than the FE simulations. As ξ decreases, the discrepancy between the analytical results and experimental tests increases, and the deviation between the theoretical and predicted simulation values also grows. In contrast, the gap between theoretical analysis and the simulation value narrows. As the thickness of the cell wall decreases, the deviation of the tested elastic constants rises gradually. The theoretical homogenized modulus E_y shows a lower stiffness at $\xi = 0.12$, which differs from the experimental value and FE simulation with an 11.71% and 5.08% gap, respectively. With the decrease of thickness, the error of theory and experiment or simulation increases gradually. For the equivalent shear modulus G_{yx}, the theoretical value is the maximum among the three results under different cell wall thicknesses. With decreasing ξ, the simulation results gradually approach the theoretical values, and the deviation is reduced from 8.36% at $\xi = 0.22$ to 1.85% at $\xi = 0.12$. Compared to the simulation results, the experimental shear moduli are from bigger to smaller with reduced cell wall thickness.

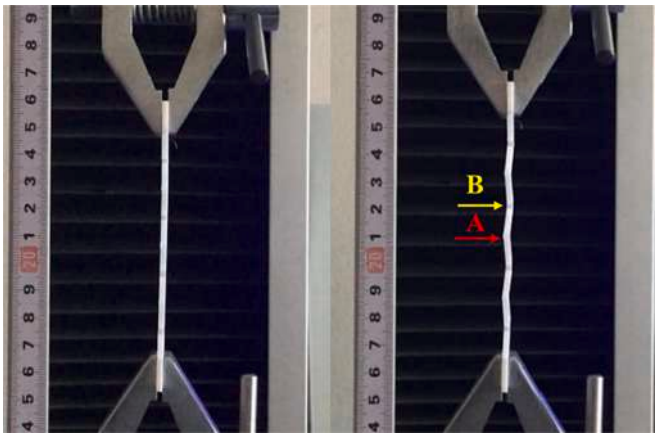

Fig. 7. Out-of-plane deformation caused by in-plane stretching: (a) original shape, (b) corrugated shape.

Uncertainties affecting the results among the three sets of data can be ascribed to a variety of reasons. The samples manufactured using the FDM technics have internal porosity and layerwise deposition, so the honeycomb material does not completely meet homogeneous and isotropic assumptions. When analyzing the homogenized tensile elastic modulus along the x direction, the inclined cell wall's contribution to the deformation of the honeycomb is neglected, causing a slight distinction between theoretical and FE results. In addition, the deformation of the horizontal cell wall under vertical tensile load increases with the decline of the cell thickness, and the assumption of ignoring the deformation of the horizontal cell wall leads to increased deviation.

It can be obtained from Table 3 that theoretical, experimental, and FE results of in-plane shear modulus with the diverse thicknesses of unit cells are relatively close to each other, the differences of which are within 10%. On the one hand, the deformation of the inclined wall caused by torque is ignored in the theoretical analysis, which is contained within the FE calculation procedure. On the other hand, the theoretical model describes the deformation of a unit cell with periodic boundary conditions in a pure shear state. However, experimental tests and FE simulation use uniaxial stretch to simulate the shear deformation and set another two surfaces free. In addition, the number of cells is also the cause of the slight difference between the three studied results.

The variation of Poisson's ratio ν_{yx} against strain for honeycombs with different wall thicknesses was obtained by FE simulation during stretching in the y-direction, as shown in Fig. 8. The Poisson's ratio is a small non-zero value. As the tensile strain increases further, the in-plane Poisson's ratio of the honeycomb structure gradually stabilizes to −0.007. The small non-zero value of Poisson's ratio can be explained by the non-uniform tensile stress of the horizontal cell walls. The internal horizontal cell walls inside the two inclined walls and the outer parts produce opposite bending deformation. The ones on the compression side are shortened, and the others on the tension side are elongated. The increasing wall thickness brings more bending resistance and more pronounced non-uniformity characteristics. The combined factors lead to a small non-zero deformation in the transverse direction.

Fig. 9 shows the comparison of the three results of out-of-plane deformation. Errors will inevitably occur in the recorded data during the test, so the deformation data of each point is recorded five times then the average value is taken. The bar chart shows that the experimental out-of-plane deformations of the three specimens are relatively consistent and are not much different from the theoretical results indicated by the square dot and FE simulation results shown by the triangle dot.

Table 3
Comparison of in-plane elastic constants of the theoretical, experimental and FE simulation results.

ξ	Equivalent modulus (MPa)	Theoretical	Experimental	FEM	Error (T-E)	Error (T-F)	Error (E-F)
0.22	E_x	233.181	239.674 ± 2.966	238.098	−2.78%	−2.11%	0.66%
	E_y	49.64	49.965 ± 2.490	51.321	−0.65%	−3.39%	−2.71%
	G_{yx}	3.431	3.233 ± 0.065	3.144	5.77%	8.36%	2.75%
0.17	E_x	184.922	191.469 ± 0.702	187.528	−3.54%	−1.41%	2.06%
	E_y	23.596	25.226 ± 0.598	24.647	−6.91%	−4.45%	2.30%
	G_{yx}	1.561	1.461 ± 0.042	1.459	6.41%	6.53%	0.14%
0.12	E_x	134.057	141.648 ± 1.826	135.063	−5.66%	−0.75%	4.65%
	E_y	8.44	9.428 ± 0.140	8.869	−11.71%	−5.08%	5.93%
	G_{yx}	0.541	0.514 ± 0.003	0.531	4.99%	1.85%	−3.31%

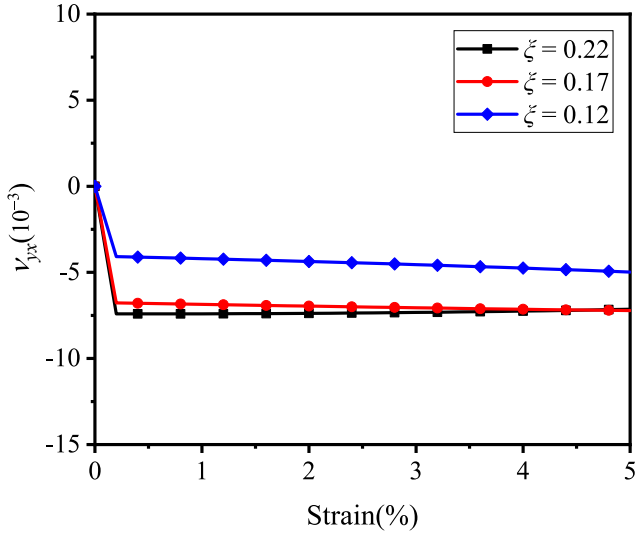

Fig. 8. The Poisson's ratio ν_{yx} against strain curve.

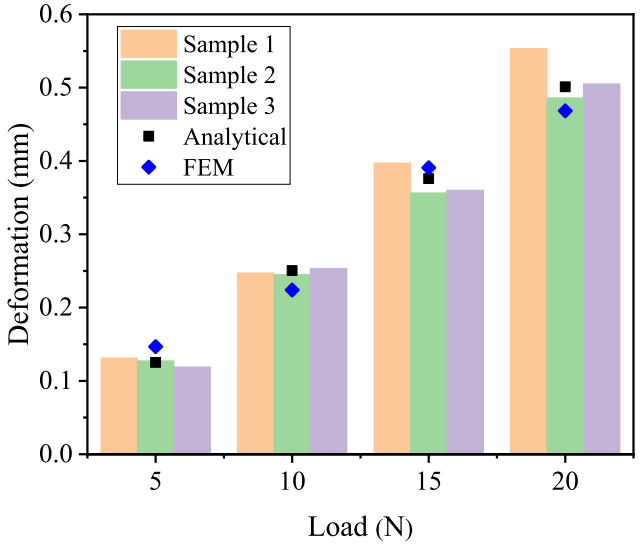

Fig. 9. Comparison of out-of-plane deformation of the theoretical, experimental and FE simulation results.

Therefore, theoretical analysis can be considered reasonable. Despite not the expected continuous arc shape, the generated local out-of-plane deformation cannot be ignored. In our future work, the material and topology of honeycombs will be designed to realize continuous bending deformation. Furthermore, the characteristic that in-plane loading actuates continuous bending deformation will be systematically investigated and demonstrated.

4. Parametric analysis

This section performs a parametric analysis of the elastic properties of the 3D deformed cellular structure to determine the dependence of the geometric parameters based on the derived equivalent modulus expression and FE simulation. The changes versus cell angle under diverse parameters of the non-dimensional modulus along the x direction of the 3D deformed honeycomb structure are plotted in Figs. 10-12, where the analyzed and simulation results are represented by solid lines and scattered points, respectively. As shown in Figs. 10-12, the theoretical results are in good agreement with the simulation results. As the angle φ increases, the simulation results are higher than the theoretical values at some points. Especially in Fig. 10, the difference between the two becomes more evident with the growing cell wall thickness. This phenomenon occurs due to the ignorance of the forces between inclined and horizontal cell walls when theoretically deriving the equivalent tensile modulus E_x. The simplification brings a larger displacement than the real one under tensile loads. Thus, theoretical values are smaller than ideal simulation results. In addition, the area where the inclined cell wall and the horizontal cell wall intersect becomes bigger as the angle φ and the parameter ξ increase, so ignoring the force influence leads to a more evident deviation between the simulation and theoretical values.

When applying a tensile load along the x direction, the horizontal cell walls significantly carry the load. Therefore, the cross-sectional parameters ξ and λ of the horizontal cell wall are the main factors affecting E_x/E_s. The 3D morphing structure is stiffer along the x direction with the increase in the cross-sectional area of the horizontal cell wall. When the parameter ξ increases from 0.1 to 0.2, E_x/E_s increases by 93%. While the parameter λ increases from 1 to 2, E_x/E_s increases by 81%. In

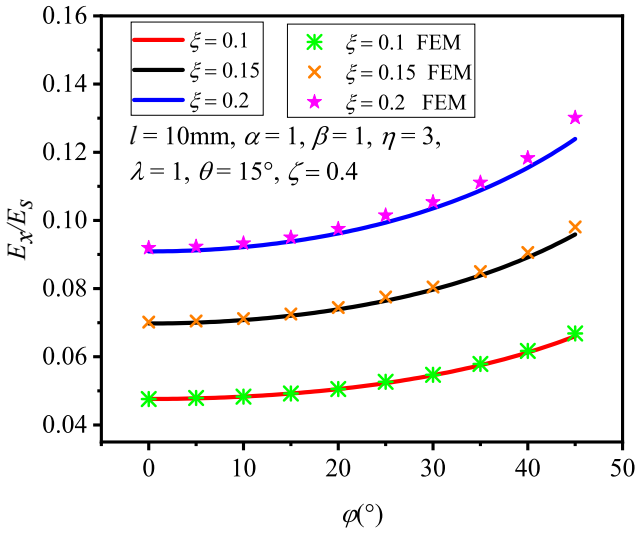

Fig. 10. Non-dimensional modulus E_x/E_s vary with the cell angles for different ξ.

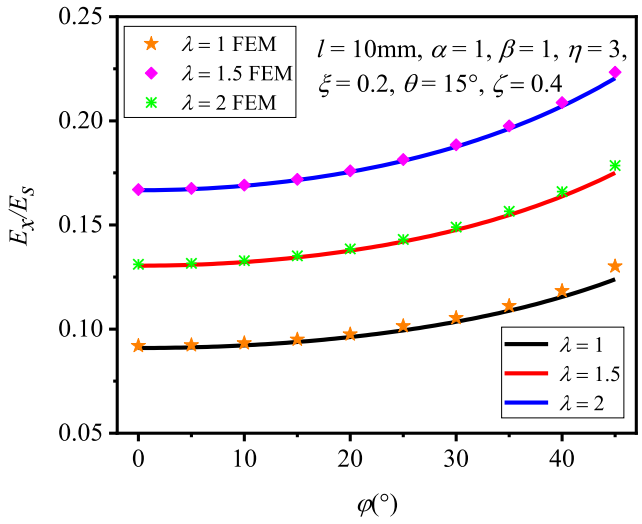

Fig. 11. Non-dimensional modulus E_x/E_s versus the cell angles for different λ.

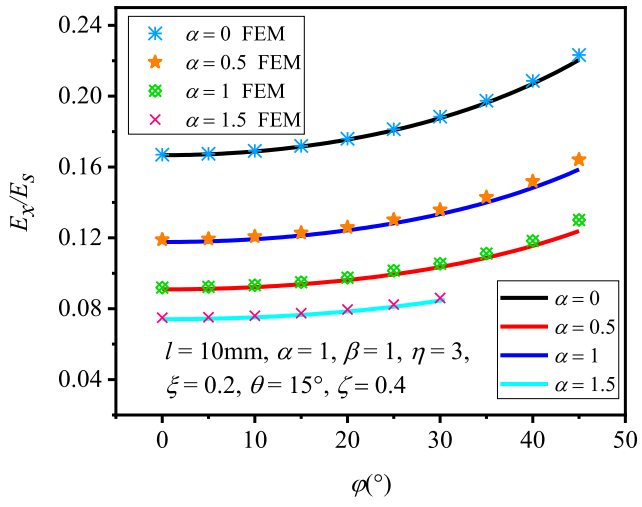

Fig. 12. Non-dimensional modulus E_x/E_s change with the cell angle for different α.

addition, the ratio of the length of the inclined cell wall to the horizontal cell wall represented by α and β also affects the equivalent modulus. From theoretical analysis, it can be considered that the effects of the two parameters are equal. Even if α and β take different values will not affect the stiffness as long as the sum of the two parameters remains unchanged. Although the morphology of the unit cell is altered by the length of the inclined cell wall, the effective cross-sectional area along the x direction is not changed, so the equivalent modulus remains consistent. Comparing the two curves with $\alpha = 0$ and $\alpha = 1$ in Fig. 12, the E_x/E_s of the latter drops significantly compared to the former. In the case of $\alpha = 0$, there is no inclined cell wall with a tilting angle, causing two adjacent horizontal cell walls to connect directly, which increases the stress cross-sectional area and stiffness.

Figs. 13-15 illustrate the relationship between the in-plane non-dimensional equivalent elastic modulus E_y/E_s and the cell angle φ of the 3D deformed honeycomb structure along the y direction under different cell geometric parameters. Similarly, the solid lines in the figure represent the theoretical results, and the scattered points denote the simulation results. The simulation result differs from the theoretical value at the cell angle equaling 0 due to the assumption that the horizontal cell wall is not deformed in the theoretical model analysis; in other words, the stiffness of the horizontal cell wall is considered close to

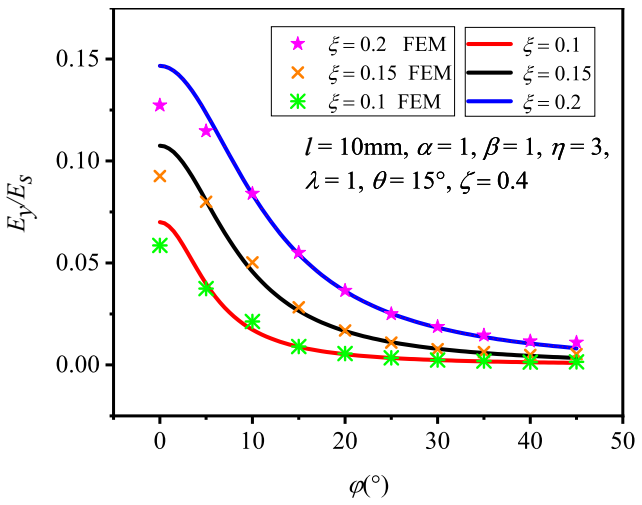

Fig. 13. Non-dimensional modulus E_y/E_s vary with the cell angles for different ξ.

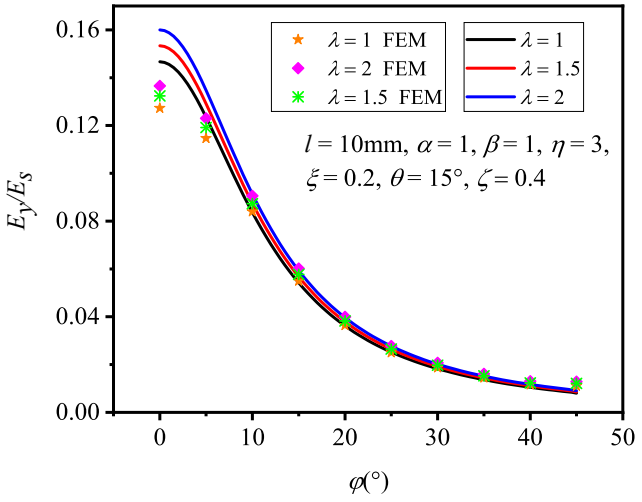

Fig. 14. Non-dimensional modulus E_y/E_s versus the cell angles for different λ.

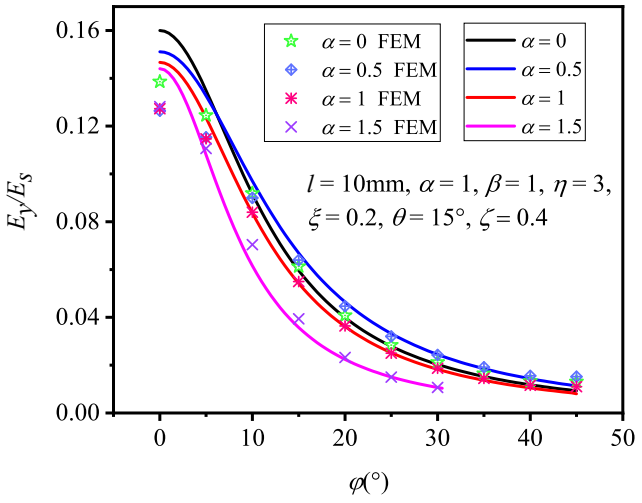

Fig. 15. Non-dimensional modulus E_y/E_s vary with the cell angle for different α.

infinity. However, the bending deformation of the horizontal cell wall is considered in the simulation calculation, resulting in the simulation result being smaller than the theoretical value. As the cell angle gradually increases, the influence caused by the deformation of the horizontal cell wall declines, and the theoretical and simulation results are in good agreement. For example, when setting the parameter $l = 10$ mm, $\alpha = 1, \beta = 1, \eta = 3, \lambda = 1, \theta = 15°, \zeta = 0.4, \xi = 0.2, \varphi = 30°$, the difference between theoretical analysis and FE calculation is 4.2%. The homogenized equivalent modulus along the y direction shows a downward trend as the angle increases under the same parameters, such as when $\xi = 0.2$, $\lambda = 1, \alpha = 1, E_y/E_s$ drops sharply as the angle φ increases from 0 to 15° by 64%. It can be seen from Fig. 13 that an increasing thickness of cell wall ξ leads to an enlargement of the in-plane non-dimensional equivalent Young's modulus E_y/E_s, which increases by 678% when ξ varies from 0.1 to 0.2 for a cell angle of 30°. Fig. 14 describes the effect of the parameter λ on E_y/E_s. It can be obtained that the thickness of the horizontal cell wall has little impact on the elastic modulus in the y direction. From the previous analysis, the parameter λ significantly influences the tensile equivalent modulus along the x direction, indicating that λ is a parameter that affects the anisotropy of the honeycomb structure. Fig. 15 shows the theoretical prediction and FE simulation calculation of the non-dimensional modulus E_y/E_s versus the cell angles with diverse parameter α. The difference caused by the parameter λ is not apparent from the overall perspective. It is worth mentioning that $\alpha = 0$ means that all inclined cell walls are perpendicular to the honeycomb surface, while $\alpha = 1$, $\beta = 1$ indicates that two types of inclined cell walls exist with the same length. The two curves are very close, indirectly showing that angle θ has little effect on the equivalent modulus along the y direction. A consistent result can be achieved by setting appropriate parameters corresponding to the geometric configurations published in reference[18].

Figs. 16-17 depict the variation of non-dimensional shear modulus G_{yx}/E_s with different geometric parameters. Although some differences exist at both ends of the curve under different conditions, the analytical solution is consistent with the trend of the homogenization simulation results. Fig. 16 shows the effect of cell wall thickness on shear modulus. As the inner angle increases, the in-plane shear modulus first falls and then goes up, and the growing cell wall thickness significantly increases the shear modulus. Fig. 17 illustrates the change of the in-plane shear modulus with parameter α, the ratio of the inclined cell wall at an angle with the honeycomb plane to the horizontal cell wall. It can be seen that shear modulus at $\alpha = 0$ is more significant than that at $\alpha = 1$, owning to the thickness of the horizontal cell wall of the former is twice that of the latter. In some cases, the shear modulus can be increased by adjusting the length of the cell wall and the cell inner angle. There are some differences between the analytical results and the FE simulation results caused by ignoring the shear force, the deformation of the horizontal cell wall, and the torque in the inclined cell wall during the theoretical analysis.

5. Conclusions

In this work, a novel cellular structure is designed and investigated, whose inclined cell walls are tilted to deviate from the original vertical plane. The designed honeycomb structure exhibits local out-of-plane deformation motivated by the in-plane tensile load. The introduced tilt angle influences the mechanical properties of the honeycomb structure with an out-of-plane internal force, which is not involved in the previous honeycomb in-plane mechanics analysis. The in-plane elastic performances of the proposed cellular structure are theoretically analyzed, including the equivalent modulus along with both horizontal and vertical directions and the equivalent shear modulus. The FE models are established to verify the rationality of the theoretical analysis. A set of experimental tests are carried out to validate the analytical and FE models. The three obtained results are generally in good agreement with each other. Furthermore, the theoretical prediction and

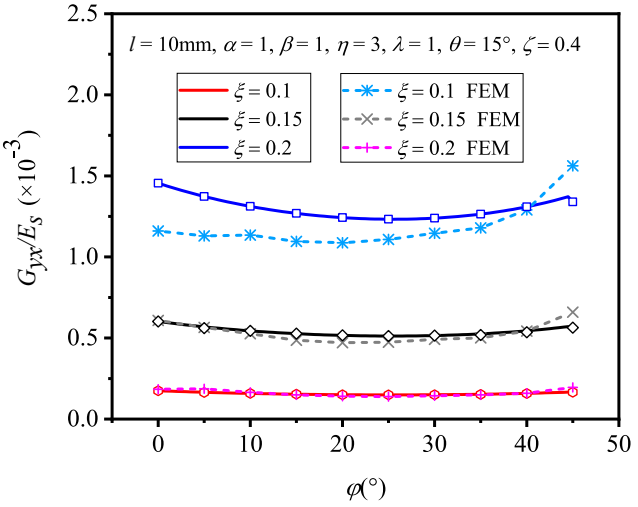

Fig. 16. Non-dimensional modulus G_{yx}/E_s vary with the cell angle for different ξ.

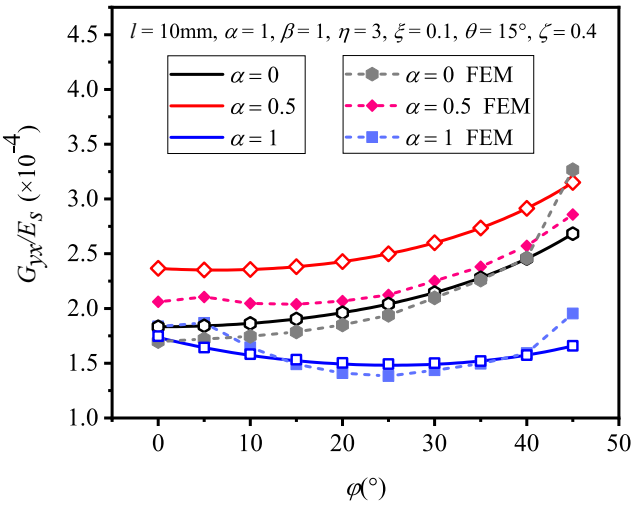

Fig. 17. Non-dimensional modulus G_{yx}/E_s vary with the cell angle for different α.

simulation methods are used to analyze the impact of cell parameters on elastic properties, showing that it is possible to acquire a wide range of mechanical performance for diverse applications by controlling the variety of the unit cell geometric parameters.

CRediT authorship contribution statement

Ting Li: Conceptualization, Investigation, Visualization, Writing – original draft, Writing – review & editing. **Jian Sun:** Conceptualization, Methodology, Supervision, Data curation, Writing – review & editing. **Jinsong Leng:** Visualization, Supervision, Writing – review & editing. **Yanju Liu:** Conceptualization, Methodology, Investigation, Writing – review & editing.

Declaration of Competing Interest

The authors declare that they have no known competing financial interests or personal relationships that could have appeared to influence the work reported in this paper.

Data availability

Data will be made available on request.

Acknowledgment

This work was supported by the National Natural Science Foundation of China (Grant No. 11802076, No. 11632005).

References

[1] Thill C, Etches J, Bond I, Potter K, Weaver P. Morphing skins. Aeronaut J 2008;112 (1129):117–39.
[2] Barbarino S, Bilgen O, Ajaj RM, Friswell MI, Inman DJ. A Review of Morphing Aircraft. J Intell Mater Syst Struct 2011;22(9):823–77.
[3] Olympio KR, Gandhi F. Zero-v Cellular Honeycomb Flexible Skins for One-Dimensional Wing Morphing. In: 48th AIAA/ASME/ASCE/AHS/ASC Structures, Structural Dynamics, and Materials Conference, Hawaii, 23-26 April 2007. p. AIAA 2007-1735.
[4] Olympio KR, Gandhi F, Asheghian L, Kudva J. Design of a Flexible Skin for a Shear Morphing Wing. J Intell Mater Syst Struct 2010;21(17):1755–70.
[5] Olympio KR, Gandhi F. Flexible Skins for Morphing Aircraft Using Cellular Honeycomb Cores. J Intell Mater Syst Struct 2009;21(17):1719–35.
[6] Olympio KR, Gandhi F. Zero Poisson's ratio cellular honeycombs for flex skins undergoing one-dimensional morphing. J Intell Mater Syst Struct 2009;21(17): 1737–53.
[7] Bubert EA, Woods BKS, Lee K, Kothera CS, Wereley NM. Design and Fabrication of a Passive 1D Morphing Aircraft Skin. J Intell Mater Syst Struct 2010;21(17): 1699–717.
[8] Gibson LJ, Ashby MF. Cellular solids: structure and properties. Cambridge, UK: Cambridge Univ. Press., 1999.
[9] Gao Q, Liao W-H, Wang L. An analytical model of cylindrical double-arrowed honeycomb with negative Poisson's ratio. Int J Mech Sci 2020;173:105400.
[10] Grima JN, Oliveri L, Attard D, Ellul B, Gatt R, Cicala G, et al. Hexagonal Honeycombs with Zero Poisson's Ratios and Enhanced Stiffness. Adv Eng Mater 2010;12(9):855–62.
[11] Bezazi A, Scarpa F, Remillat C. A novel centresymmetric honeycomb composite structure. Compos Struct 2005;71(3–4):356–64.
[12] Harkati A, Boutagouga D, Harkati E, Bezazi A, Scarpa F, Ouisse M. In-plane elastic constants of a new curved cell walls honeycomb concept. Thin-Walled Struct 2020; 149:106613.
[13] Liu W, Li H, Zhang J, Li H. Elastic properties of a novel cellular structure with trapezoidal beams. Aerosp Sci Technol 2018;75:315–28.
[14] Liu W, Li H, Zhang J, Li H. Theoretical analysis on the elasticity of a novel accordion cellular honeycomb core with in-plane curved beams. J Sandw Struct Mater 2018;22(3):702–27.
[15] Gong X, Huang J, Scarpa F, Liu Y, Leng J. Zero Poisson's ratio cellular structure for two-dimensional morphing applications. Compos Struct 2015;134:384–92.
[16] Liu W, Li H, Zhang J, Bai Y. In-plane mechanics of a novel cellular structure for multiple morphing applications. Compos Struct 2019;207:598–611.
[17] Liu W, Li H, Zhang J, Gong X, Wang Y, Ge X. Tensile and shear properties of star-shaped cellular lattice structure. Mech Adv Mater Struct 2021;28(24):2605–17.
[18] Huang J, Gong X, Zhang Q, Scarpa F, Liu Y, Leng J. In-plane mechanics of a novel zero Poisson's ratio honeycomb core. Compos B Eng 2016;89:67–76.
[19] Huang J, Zhang Q, Scarpa F, Liu Y, Leng J. In-plane elasticity of a novel auxetic honeycomb design. Compos B Eng 2017;110:72–82.
[20] Liu W, Li H, Yang Z, Zhang J, Ge X. In-plane elastic properties of a 2D chiral cellular structure with V-shaped wings. Eng Struct 2020;210:110384.
[21] Chen YJ, Scarpa F, Liu YJ, Leng JS. Elasticity of anti-tetrachiral anisotropic lattices. Int J Solids Struct 2013;50(6):996–1004.
[22] Günaydın K, Eren Z, Kazancı Z, Scarpa F, Grande AM, Türkmen HS. In-plane compression behavior of anti-tetrachiral and re-entrant lattices. Smart Mater Struct 2019;28(11):115028.
[23] Alderson A, Alderson KL, Attard D, Evans KE, Gatt R, Grima JN, et al. Elastic constants of 3-, 4- and 6-connected chiral and anti-chiral honeycombs subject to uniaxial in-plane loading. Compos Sci Technol 2010;70(7):1042–8.
[24] Harkati E, Daoudi N, Bezazi A, Haddad A, Scarpa F. In-plane elasticity of a multi re-entrant auxetic honeycomb. Compos Struct 2017;180:130–9.
[25] Hu LL, Luo ZR, Zhang ZY, Lian MK, Huang LS. Mechanical property of re-entrant anti-trichiral honeycombs under large deformation. Compos B Eng 2019;163: 107–20.
[26] Peng X-L, Bargmann S. A novel hybrid-honeycomb structure: Enhanced stiffness, tunable auxeticity and negative thermal expansion. Int J Mech Sci 2021;190: 106021.
[27] Xu M, Liu D, Wang P, Zhang Z, Jia H, Lei H, et al. In-plane compression behavior of hybrid honeycomb metastructures: Theoretical and experimental studies. Aerosp Sci Technol 2020;106:106081.
[28] Huang J, Zhang Q, Scarpa F, Liu Y, Leng J. Shape memory polymer-based hybrid honeycomb structures with zero Poisson's ratio and variable stiffness. Compos Struct 2017;179:437–43.
[29] Ingrole A, Hao A, Liang R. Design and modeling of auxetic and hybrid honeycomb structures for in-plane property enhancement. Mater Des 2017;117:72–83.
[30] Alderson A, Alderson KL, Chirima G, Ravirala N, Zied KM. The in-plane linear elastic constants and out-of-plane bending of 3-coordinated ligament and cylinder-ligament honeycombs. Compos Sci Technol 2010;70(7):1034–41.
[31] Bishay PL, Finden R, Recinos S, Alas C, Lopez E, Aslanpour D, et al. Development of an SMA-based camber morphing UAV tail core design. Smart Mater Struct 2019;28 (7):075024.
[32] Emiliavaca A, de Araújo CJ, Souto CR, Ries A. Characterization of shape memory alloy micro-springs for application in morphing wings. Smart Mater Struct 2019;28 (1):015010.
[33] Hajarian A, Zakerzadeh MR, Baghani M. Design, analysis and testing of a smart morphing airfoil actuated by SMA wires. Smart Mater Struct 2019;28(11):115043.
[34] Sales TD, Rade DA, Inman DJ. A morphing metastructure concept combining shape memory alloy wires and permanent magnets for multistable behavior. J Braz Soc Mech Sci Eng 2020;42(3):122.
[35] Ou J, Ma Z, Peters J, Dai S, Vlavianos N, Ishii H. KinetiX - designing auxetic-inspired deformable material structures. Comput Graph 2018;75:72–81.
[36] Ott V, Keidel D, Kölbl M, Ermanni P. Investigation of an adaptive, hinge-less, and highly shear stiff structure for morphing skins. J Intell Mater Syst Struct 2019;31 (3):445–56.